INTERNATIONAL JOURNAL FOR NUMERICAL METHODS IN FLUIDS
Int. J. Numer. Meth. Fluids **29**: 411–427 (1999)

COMPUTATIONS OF A LAMINAR BACKWARD-FACING STEP FLOW AT $Re = 800$ WITH A SPECTRAL DOMAIN DECOMPOSITION METHOD

JAYANT KESKAR*,[1] AND D.A. LYN

School of Civil Engineering, Purdue University, West Lafayette, IN 47907, USA

SUMMARY

The two-dimensional laminar incompressible flow over a backward-facing step is computed using a spectral domain decomposition approach. A minimum number of subdomains (two) is used; high resolution being achieved by increasing the order of the basis Chebyshev polynomial. Results for the case of a Reynolds number of 800 are presented and compared in detail with benchmark computations. Stable accurate steady flow solutions were obtained using substantially fewer nodes than in previously reported simulations. In addition, the problem of outflow boundary conditions was examined on a shortened domain. Because of their more global nature, spectral methods are particularly sensitive to imposed boundary conditions, which may be exploited in examining the effect of artificial (non-physical) outflow boundary conditions. Two widely used set of conditions were tested: pseudo stress-free conditions and zero normal gradient conditions. Contrary to previous results using the finite volume approach, the latter is found to yield a qualitatively erroneous yet stable flow-field. Copyright © 1999 John Wiley & Sons, Ltd.

KEY WORDS: spectral domain decomposition method; laminar incompressible backward-facing step flow

1. INTRODUCTION AND REVIEW

The two-dimensional laminar incompressible flow over a backward-facing step (BFS) is a canonical example of a separated flow with reattachment, and the relative simplicity of its numerical formulation has made it popular as a benchmark case. Although it has received much attention, it still poses challenges, or at least traps, for the unwary analyst, as evidenced in the recent controversy regarding the flow at a Reynolds number (based on channel height and average channel velocity) of $Re = 800$. Kaiksis *et al.* [1] computed this flow using the spectral element method, which might be viewed as a finite element approach using high-order 'spectral' basis functions rather than the more conventional low-order polynomials. They argued that the flow at $Re = 800$ is unsteady and exhibited chaotic behavior. A similar conclusion was also reached in studies using unsteady finite volume approaches [2,3]. This however, conflicted with benchmark finite element computations [4], computed assuming a steady flow. A collaborative effort [5] (hereafter referred to as G93) reconsidered this problem using a variety of methods, and found that, even when a transient simulation was performed, the BFS flow at $Re = 800$ was stable and steady. The most convincing case was presented by

* Correspondence to: School of Civil Engineering, Purdue University, West Lafayette, IN 47907, USA.
[1] Current address: AGA Computer Services Inc., Tampa, FL 33619, USA.

CCC 0271–2091/99/040411–17$17.50

Received 29 September 1997
Revised 31 March 1998

repeating the computations with a spectral element code very similar to that used by Kaiksis *et al.* [1], and finding that the flow was underresolved with the Kaiksis *et al.* 'grid', and that, through the use of a more refined grid, a steady flow was achieved (see also Torczynski [6]).

The present work was motivated in part by the above controversy and its implications for the use of spectral methods with domain decomposition (the spectral element approach being only one of several spectral domain decomposition methods). The results of G93 with the spectral element method suggested that quite a fine spectral grid, more comparable with conventional finite element meshes, was necessary in order to fully resolve the flow. This makes the spectral approach correspondingly less attractive for high resolution computations in comparison with more conventional approaches. Doubt was cast on the 'exponential' accuracy of spectral methods (its main advantage in comparison with more common methods) when applied to the BFS flow. A possible explanation, the presence of a singularity at the step, was offered, since exponential accuracy is guaranteed only for 'smooth' solutions, and the presence of singularities will degrade the solution obtained by a spectral method. The aspect ratio of the elements was also singled out as a measure of grid refinement. On the most refined grid, the aspect ratio of the elements was restricted to a maximum value of 2, contrasting with a maximum value of 10 in the Kaiksis *et al.* grid.

A modified version of the pseudo spectral matrix element (PSME) method [7] is applied in the present work to the BFS flow. A steady flow solution for $Re = 800$ was obtained with even fewer nodes than was used in the Kaiksis *et al.* grid, which was found inadequate in G93. In addition, the problem of outflow or open boundary conditions (OBCs) is considered. The benchmark computations of the BFS flow at $Re = 800$ were in fact originally intended for use in a mini-symposium on OBCs [8]. Because of their more global high-order nature (compared with conventional finite difference or finite element methods), spectral methods can be quite sensitive to boundary conditions [9], and therefore, especially appropriate for a study of OBCs. In the recent OBC mini-symposium, only a single contribution used a spectral method, namely a spectral element approach the results of which have since been proven unreliable.

2. PROBLEM STATEMENT

2.1. Basic equations

The equation for unsteady two-dimensional laminar incompressible flow expressing the conservation of momentum is commonly formulated in dimensionless primitive variable form as:

$$\frac{\partial \mathbf{u}}{\partial t} + \mathbf{u} \cdot \nabla \mathbf{u} = -\nabla p + \frac{1}{Re} \nabla^2 \mathbf{u}, \tag{1}$$

where $\mathbf{u} = (u, v)$ are velocity components in the Cartesian co-ordinate directions (x, y), p is the kinematic pressure, and t is the time. In addition, the incompressibility constraint or continuity equation,

$$\nabla \cdot \mathbf{u} = 0, \tag{2}$$

must also be satisfied. Whereas Equation (1) is applied in the interior of the domain, Equation (2) must be applied in both the interior *and* the boundary of the domain.

2.2. Alternate equations

There is some empirical numerical evidence [10] that an alternate form of Equation (1), the skew-symmetric form, namely,

$$\frac{\partial \mathbf{u}}{\partial t} = -\nabla p - \frac{1}{2}[\nabla \cdot (\mathbf{uu}) + \mathbf{u} \cdot \nabla \mathbf{u}] + \frac{1}{Re}\nabla^2 \mathbf{u} = -\nabla p - F(\mathbf{u}), \tag{3}$$

may have certain advantages in spectral computations, and hence, this form was used in the actual computations. Here, $F(\mathbf{u})$ represents the advection and diffusive terms, but excludes the pressure term.

If the divergence of (1) is taken, then a Poisson equation for the pressure field or a continuous pressure-Poisson equation (PPE) results, namely,

$$\nabla^2 p = -\left[\frac{\partial}{\partial t}(\nabla \cdot \mathbf{u}) + \nabla \cdot (\mathbf{u} \cdot \nabla \mathbf{u}) - \frac{1}{Re}\nabla \cdot (\nabla^2 \mathbf{u})\right] = -\nabla \cdot (\mathbf{u} \cdot \nabla \mathbf{u}). \tag{4}$$

The right-hand-side of the first equality, with the unsteady term set to zero, has been termed the consistent PPE [11] to distinguish it from the second equality, in which Equation (2) has been applied throughout. The latter equation has been widely used in numerical solutions of incompressible flow, and has generated much discussion, especially with regards to the appropriate boundary conditions. Gresho and Sani [11] have argued that, for a problem in which only Dirichlet velocity boundary conditions are imposed, no additional boundary condition for p is necessary. In a numerical solution of the PPE, however, a boundary condition must be imposed, and they asserted that the normal momentum equation,

$$\mathbf{n} \cdot \left[\frac{\partial \mathbf{u}}{\partial t} + \mathbf{u} \cdot \nabla \mathbf{u} + \nabla p - \frac{1}{Re}\nabla^2 \mathbf{u}\right] = 0, \tag{5}$$

is the appropriate boundary condition for Equation (4) wherever a Dirichlet condition on velocity is imposed.

2.3. Computational domain and initial and boundary conditions

The step geometry chosen for the study has a step height of $\frac{1}{2}$ and a channel height of 1 (Figure 1). The solution domain corresponds to the geometry of the benchmark case of Gartling [4], namely, a section of total length 30 downstream of the step with no section

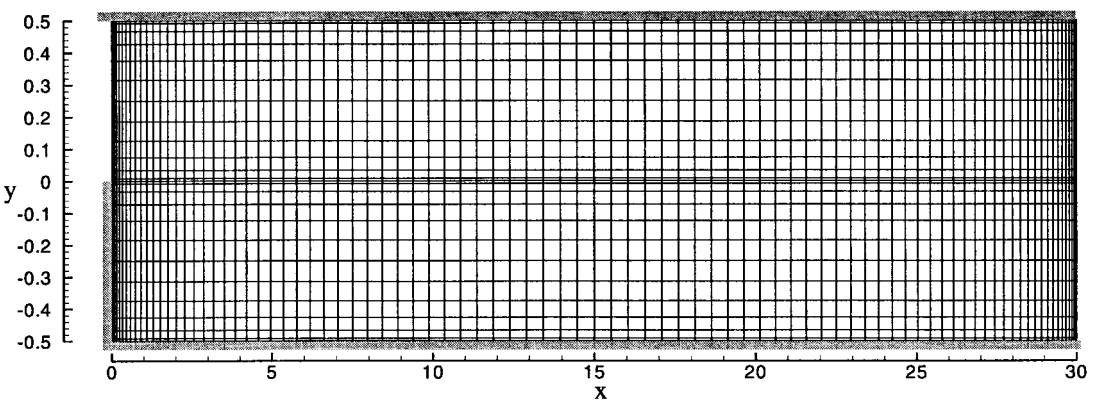

Figure 1. Computational domain and grid.

upstream of the step. In the study of outflow conditions, the computational domain downstream of the step is shortened to a length of 7. This length was chosen by the organizers of the OBC mini-symposium [8], since a recirculation region is thereby truncated, and hence severely tests the ability of an OBC to allow flow to return into the truncated domain.

The governing differential equations must be completed by boundary conditions. On the stationary solid walls, the no-slip condition ($\mathbf{u} = 0$) is imposed, while at the inlet, a parabolic velocity profile is specified, i.e. $u(x = 0,\ y \geq 0) = 24y(\frac{1}{2} - y)$, $v(x = 0,\ y \geq 0) = 0$. u is continuous at the inlet, but its cross-stream gradient is not, such that a weak singularity is present. On the other hand, v is smooth, being identically equal to zero throughout $x = 0$.

For computations done over the entire domain (the full-domain case), the pseudo stress-free condition,

$$-p + \frac{1}{Re}\frac{\partial u}{\partial x} = 0 \quad \text{and} \quad \frac{\partial v}{\partial x} = 0, \tag{6}$$

is applied at the outlet. This condition is popular among finite element practitioners, since it arises as the natural boundary condition when the viscous stress term is formulated as in Equation (1). Sani and Gresho [8] remarked that, although its physical interpretation is not clear, Equation (6) is preferable to the true stress-free condition

$$-p + \frac{2}{Re}\frac{\partial u}{\partial x} = 0, \tag{7a}$$

$$\frac{\partial u}{\partial y} + \frac{\partial v}{\partial x} = 0, \tag{7b}$$

because the latter, particularly Equation (7b), tends to be too restrictive for most flows, since stresses do not necessarily all vanish at an outflow boundary. In his finite element benchmark solution, Gartling [4] imposed hybrid outlet conditions ($v = 0$ and Equation (7a)). Since the outlet at $x = 30$ is sufficiently far from the step, the flow has essentially relaxed to a parallel uniform flow with a fully developed parabolic velocity profile, such that Equation (6) becomes equivalent to the outlet conditions of Gartling.

2.4. Outflow boundary conditions (OBCs)

Because of their more global nature, spectral methods tend to be more sensitive to imposed boundary conditions [9,12]. Domain decomposition in spectral methods has specifically been considered as a means of reducing this sensitivity. Schumack *et al.* [13] examined the use of multiple domains in isolating boundary singularities in a cavity flow, so as to reduce their effect on spectral simulations in regions away from the singularities. Separate domains at the outlet, which could act as a buffer, have also enjoyed popularity [1,12]. Though from a practical viewpoint, the sensitivity to boundary conditions may be a disadvantage, it may be exploited in studying outflow boundary conditions since effects that may apparently be negligible when conventional, more local methods are applied, may be amplified. In the present work with only two domains, nodes at the outlet boundary are directly connected through the interpolating polynomial to nodes at the inlet plane. As such, distorting effects at the outlet due to imperfectly transmitting boundary conditions are more likely to be communicated throughout the domain.

In the study of outflow boundary conditions, two other conditions, in addition to Equation (6) were considered. The zero normal gradient condition,

$$\frac{\partial \mathbf{u}}{\partial t} = 0, \tag{8}$$

is frequently used in finite difference and finite volume simulations when the outlet is placed in a region far from any flow feature of interest. Though Sani and Gresho [8] argued that this condition may yield an ill-posed problem, a number of (finite difference/finite volume) contributors to the mini-symposium on OBCs applied it successfully to the BFS flow, one even arguing that it performed better than Equation (6).

The 'radiation' or convective boundary condition

$$\frac{\partial \mathbf{u}}{\partial t} + U_c \frac{\partial \mathbf{u}}{\partial x} = 0 \tag{9}$$

has recently become popular (again primarily in the finite difference and finite volume world), especially in transient problems with flow features, such as vortices that must leave the computational domain with minimum distortion. Here, U_c is a convection velocity associated with such features, which is usually not known *a priori*. Again, while Sani and Gresho [8] note that this condition also may yield an ill-posed problem, it was used with some success by at least one of the contributors to the OBC mini-symposium. For a steady flow, the application of the radiation condition should revert to the simple zero normal gradient conditions (Equation (8)) when the steady state is approached. In an 'explicit' implementation ($\mathbf{u}^{n+1} = \mathbf{u}^n - U_c(\partial \mathbf{u}^n/\partial x)$), this OBC reduces to a Dirichlet specification of the velocity at the outlet, which, as will be seen, is especially simple to implement in the present approach. It proved however, unstable for the BFS problem, for which the following explanation may be offered. The incompressibility constraint and the no-slip condition along the channel top and bottom boundaries together imply that $\partial v/\partial y = 0$ at the channel boundaries. If however, the velocity profile at the outlet is already specified (through a Dirichlet condition based on an explicitly implemented radiation condition), then this overspecification gives rise to an inconsistency, leading to an explosive instability. An implicit implementation of the radiation condition was also tested, but was not more successful. This condition was however, applied 'successfully' to the external unconfined unsteady flow around a square cylinder.

3. THE NUMERICAL APPROACH

The basic PSME solution algorithm is a multidomain primitive variable Chebyshev collocation technique, in which the velocity and pressure fields are expanded in equal-order Chebyshev polynomials, $T_n(x)$ or $T_m(y)$, on Gauss–Lobatto collocation points, i.e. including endpoints. The incompressibility constraint is enforced via a projection scheme and velocity boundary conditions are satisfied exactly. It is described fully in Ku *et al.* [7], and so only the essential aspects are given here. Gresho [14] emphasized the importance of satisfying the incompressibility constraint in the solution of the governing equations. In G93, the spectral element method applied to the BFS flow was found to satisfy overall continuity over an element, but local divergences within elements were large if spatial resolution was insufficient. Recognizing the importance of the incompressibility constraint, the PSME approach enforces incompressibility at all nodes, including all domain and subdomain boundary nodes. At subdomain interfaces, the method directly imposes the incompressibility constraint rather than explicitly imposing the continuity of the first derivative (continuity of the function itself is obtained by construction). Like the spectral element method, continuity of the first derivative is imposed only implicitly, and is satisfied exactly only in the limit as the order of the basis polynomial tends to infinity.

3.1. The projection scheme

The projection scheme assumes the velocity at the $(n+1)$th time step at any point to be of the form,

$$\mathbf{u}^{n+1} = \bar{\mathbf{u}}^{n+1} - \Delta t \nabla \tilde{p}, \tag{10}$$

where Δt is the time step, and $\bar{\mathbf{u}} = (\bar{u}, \bar{v})$ are intermediate 'predicted' velocities. The time level of $\tilde{p}$ will be discussed below. In the domain interior, $\bar{\mathbf{u}}$ are obtained from an explicit first-order approximation to the unsteady momentum equation *without* the pressure-gradient term,

$$\frac{\bar{\mathbf{u}}^{n+1} - \mathbf{u}^n}{\Delta t} = F(\mathbf{u}^n). \tag{11}$$

In the correction step, the intermediate velocity solution is projected onto a divergence-free space by requiring that $\mathbf{u}^{n+1}$ satisfy the incompressibility constraint. The result is the well-known semi-discrete pressure-Poisson equation,

$$\nabla \cdot \mathbf{u}^{n+1} = -\nabla^2 \tilde{p} + \frac{1}{\Delta t} \nabla \cdot \bar{\mathbf{u}}^{n+1} = 0, \tag{12}$$

for $\tilde{p}$. With a solution for $\tilde{p}$, a divergence-free velocity field can be obtained by updating with Equation (10). Because the momentum equation is applied only *within* the domain, $\bar{\mathbf{u}}^{n+1}$ is determined through Equation (11) only within the domain and *not* on the boundary.

3.2. The original and the modified PSME approach

The question of the appropriate boundary condition to be applied in the solution of Equation (12) must be addressed. Whereas other approaches based on a PPE typically seek to impose a boundary condition on p (here $\tilde{p}$), the PSME approach directly enforces the incompressibility constraint on the boundary, i.e. the PPE (Equation (12)) is also applied on the boundary. For a Dirichlet problem, the ill-posedness of applying the differential equation on the boundary is resolved by eliminating the combination of $\bar{\mathbf{u}}^{n+1}$ and $\tilde{p}$ in favor of known boundary values of $\mathbf{u}^{n+1}$ using Equation (10) everywhere on the boundary in the assembly of the linear system *before* it is solved. The problem of spurious pressure oscillation, also associated with the treatment of boundary points, introduces other complications, as is elaborated below. In this respect, it resembles the familiar static condensation procedure. Thus, the exact velocity boundary conditions provide effective 'boundary conditions' for the PPE, which becomes solvable without invoking boundary conditions on $\tilde{p}$. This is entirely in accord with the claim [11] that Dirichlet velocity conditions are sufficient for the numerical solution of Equations (1) and (2). The original formulation of the PSME approach is straightforward in implementation when Dirichlet conditions on $\mathbf{u}$ are imposed. For general boundary conditions, involving velocity gradients (and possibly pressure), velocities are not known on the boundary and so cannot be used to analytically modify the PPE at the boundary nodes and thus obtain a solvable system.

In order to accommodate a variety of boundary conditions, a modification of the original PSME method was undertaken. The explicit step in the treatment of the momentum equation in the interior *cannot* enforce velocity boundary conditions. This does not present a problem for Dirichlet velocity conditions, since velocities are known at the boundaries. In the PSME approach, all boundary conditions, including those on the velocity, must be enforced in the solution of the discrete PPE. The PPE is still applied at every node, including those at the boundary, but, instead of incorporating immediately known (Dirichlet) boundary values of $\mathbf{u}$,

the resulting system of equations is augmented by additional auxiliary equations enforcing the velocity boundary conditions, somewhat similar to a spectral tau method [9,15]. Additional equations require however, additional unknowns, and the question arises as to which 'unknowns' are available. For a two-dimensional problem, at each boundary node, three conditions need to be satisfied: one due to the incompressibility constraint and two others generally imposed on the velocity (and possibly also involving the pressure), such as no-slip conditions.

One unknown is $\tilde{p}$, but two others must be found. The intermediate variable, $\bar{\mathbf{u}}$, is obtained from the momentum equations only in the interior of the domain, and are undetermined on the boundary. The undetermined boundary values of $\bar{\mathbf{u}} = (\bar{u}, \bar{v})$ provide precisely the required number of unknowns. In the simple case of Dirichlet boundary conditions on velocity, these unknowns need not be explicitly used, but an examination of the PSME 'condensation' procedure for treating Dirichlet velocity conditions may be interpreted as an *analytic* elimination of unknowns (including $\bar{\mathbf{u}}$). The use of $\bar{\mathbf{u}}$ and $\tilde{p}$ in additional equations for boundary values represents an entirely equivalent numerical elimination procedure. Thus, at each boundary node, three boundary conditions are matched with three unknowns, $(\tilde{p}, \bar{u}^{n+1}, \bar{v}^{n+1})$. In the current implementation of the algorithm, further economy is achieved by using Equation (10) to eliminate the unknown intermediate velocity variables in favor of unknown $\mathbf{u}_{\mathrm{nD}}^{n+1}$ at boundary points where non-Dirichlet conditions are imposed, and known $\mathbf{u}_{\mathrm{D}}^{n+1}$ where Dirichlet conditions are imposed. Thus, an 'augmented' PPE in matrix form,

$$A\begin{bmatrix} \tilde{p} \\ \mathbf{u}_{\mathrm{nD}}^{n+1} \end{bmatrix} = b, \tag{13}$$

is solved in which $\tilde{p}$ is a vector of length N_{tot} equal to the total number of nodes (including boundary nodes), and $\mathbf{u}_{\mathrm{nD}}^{n+1}$ is a vector of length $2N_{\mathrm{nD}}$, where N_{nD} is the total number of boundary nodes where non-Dirichlet conditions are imposed. The elements of the matrix A are obtained from the elements of Chebyshev collocation first and second derivative matrices, while the vector b is obtained from the already computed values of $\bar{\mathbf{u}}$ in the interior of the domain *and*, at (velocity) Dirichlet boundary points, the known boundary values, $\mathbf{u}_{\mathrm{nD}}^{n+1}$.

Computations were also attempted with the normal momentum equations (Equation (5)) as boundary conditions for the PPE. In the case of a regularized cavity flow, the solution obtained was divergence-free in the domain interior, but small non-zero divergences were observed on the boundary. These remained localized on the boundary and did not lead to any computational instability. On the other hand, in the benchmark BFS flow, additional problems with the use of Equation (5) arise due to the discontinuity of the cross-stream velocity gradient at the step. Boundary divergence becomes quite substantial, and, at least with the present method, eventually led to explosive instability. The normal momentum equation as boundary condition would seem to require more smoothness than the original continuity equation (which does not involve $\partial u/\partial y$). Similar problems when imposing Equation (5) as a boundary condition have been reported for fractional step methods [12].

3.3. The time level of $\tilde{p}$

Substitution of Equation (11) into Equation (12) yields a PPE directly in terms of $\mathbf{u}^n$ as

$$\nabla^2\tilde{p} = -\left[\frac{1}{\Delta t}(\nabla\cdot\mathbf{u}^n) + \nabla\cdot(\mathbf{u}^n\nabla\cdot\mathbf{u}^n) - \frac{1}{Re}\nabla\cdot(\nabla^2\mathbf{u}^n)\right], \tag{14}$$

which is seen to be a form of the consistent PPE (Equation (4)). Gresho [14] has argued that, since the pressure is always in equilibrium with the associated velocity field and the velocity field on the right-hand-side of Equation (14) is evaluated at time level, n, then $\tilde{p} = p^n$. From this perspective, the scheme is viewed as a simple forward Euler method. If the boundary condition applied to Equation (14) were derived from the normal momentum equation (Equation (5)) with velocity terms evaluated at the nth time level, then this argument would be clearly applicable. In the present approach, however, although Equation (14) is applied in the interior of the domain, the imposed boundary conditions involves velocities (in the case of Dirichlet conditions, known, and in the case of non-Dirichlet conditions, unknown) at the $(n+1)$th time level. As such, the time level of $\tilde{p}$ is ambiguous in this regard, similar to the semi-implicit scheme of Chorin [16], and should be interpreted as the pressure at an intermediate time, or as a first-order (in time) estimate of p^{n+1} (or for that matter, p^n) [17]. Also, the scheme cannot be strictly characterized as simple forward Euler because of the implicit treatment of the boundary nodes. For the present problem, in which the flow is expected to relax to a steady state, the time level of $\tilde{p}$ will be of no consequence.

3.4. Strategies in spectral domain decomposition

In conventional finite element or finite volume techniques, grid refinement is typically achieved by increasing the number of elements or cells. Whereas with global spectral methods, grid refinement is accomplished by increasing the order (N_x or N_y) of the basis polynomial, with spectral domain decomposition approaches, both strategies can be considered. Kaiksis *et al.* [1] and the spectral element solution in G3 considered mainly the option of increasing the number of subdomains, though the effect of increasing the order of the basis polynomial was also studied. In the simulation of the BFS at $Re = 800$, Kaiksis *et al.* used 44 subdomains with most results being obtained with $N_x = N_y = 8$, while the finest grid in the spectral element simulation in G3 used 136 subdomains, with $N_x = N_y = 8$. The present work examines the alternative strategy, that of minimizing the number of subdomains and obtaining higher resolution by means of increasing the order of the basis polynomials. Although the problem domain is very regular, being a simple rectangle, the step at the inlet with its associated boundary condition dictates that the minimum number of subdomains appropriate for the BFS flow is two. All computations reported below were performed with two subdomains. Because of the large aspect ratio (channel length/channel height) for such subdomains, it might be expected that, in contrast to the choice made in previous spectral element studies, the order of the polynomial in the streamwise direction, N_x, may need to be much larger than that in the cross-stream direction, N_y.

3.5. Some numerical details

Computations were started with zero initial conditions everywhere in the interior of the domain. No problem was encountered with the ill-posedness of the initial data, which does not satisfy the divergence-free condition. Gresho [14] has noted that a backward Euler or the semi-implicit projection scheme of Chorin [16] converts any initial velocity field into a divergence-free field after the initial time step. Although the present scheme treats the nodes in the interior in an explicit fashion, a divergence-free solution was obtained after the first time step, which is attributed to the implicit treatment of boundary points. Though the initial pressure might be unphysical, this is of no consequence in the final steady state. The computations were marched in time until a steady state was achieved; no parameter marching (starting at low Re and increasing Re during computations) was performed. Because of the

explicit treatment of the momentum equations in the domain interior, the time step for numerical stability, $(\Delta t)_{\text{crit}}$ is limited by both a Courant condition ($(\Delta t)_{\text{crit}} \sim (\Delta s)_{\min}/U_{\max}$) as well as a diffusion condition, $(\Delta t)_{\text{crit}} \sim Re(\Delta s)^2_{\min}$, where Δs refers to either Δx or Δy. For high Re problems, the Courant condition tends to be more restrictive [7], as was found to be the case in the present work where $Re = 800$. The time step was chosen to be just below the stability limit (e.g. $\Delta t = 0.002$ for the $Re = 800$, full-domain case with $N_x = 90$ and $N_y = 12$), since interest was focused on the final steady state. Computations were terminated when the solution at two different times ($t_2 - t_1 = 1$) did not differ significantly, measured by the L_1 norm, viz. $\Sigma\,|f(t_2) - f(t_1)| < 2 \times 10^{-5}$, where the sum is taken over all nodes, and f is either u or v. Computations were performed until at least $t = 700$ for the full-domain case; the time taken to satisfy the termination criterion was significantly less for the short-domain case, and hence these computations were terminated at $t = 400$.

A standard LU decomposition is performed on the matrix A in Equation (13), and the solution at each time step is obtained using the already factorized matrix by matrix multiplication. Because the time integration is quite long, the factorization step is negligible compared with the time marching step. All computations were done in 32-bit precision on various models of IBM/RS6000 workstations. On a Model 595, the factorization step for the ($N_x = 90$, $N_y = 12$) simulation required ≈ 130 s of CPU time, while each time step required ≈ 1 s of CPU time. No special compiler optimization directives were specified.

An attractive feature of spectral methods is that the derived quantities involving derivatives or integrals of the primitive variables, such as the vorticity, $\omega \equiv (\partial v/\partial x - \partial u/\partial y)$, or the streamfunction, $\Phi = \int_{\mathscr{L}} u\,\mathrm{d}y$, can be evaluated with 'spectral' accuracy because the high-order approximating polynomial can be recovered from nodal values. Thus, provided the solution is smooth and well-resolved, these quantities will share the asymptotic exponential accuracy of the solution. For the same reason, interpolation of values between nodes can also be performed accurately. This is particularly important if much fewer, and hence much more widely spaced, nodes are possible with spectral methods. For example, in addition to the local divergence ($\nabla \cdot \mathbf{u}$) being zero (to machine accuracy) at nodes by construction; the interpolated divergence is also zero ($O(10^{-10})$). All derived quantities in the following are spectrally evaluated and considerable use is made of spectral interpolation. Thus, whereas Gartling [4] evaluated derivatives at the 2×2 Gauss points and projected these to corner nodes by bilinear extrapolation, as well as linearly interpolated nodal shear stresses to identify separation and reattachment points, the present work evaluated derivatives and interpolated from a high-order (either of order N_x or N_y except in the case of pressure field where the order is reduced, see below) polynomial.

The non-staggered arrangement of the variables, combined with the imposition of the incompressibility on the boundary, gives rise to spurious oscillations in the pressure field [15,18] due to the use of modes with pressure gradients identically zero at all collocation points where the momentum equation is enforced. Pressure gradients at the collocation points in the interior of the domain, where the momentum equations are enforced are however, computed correctly, so that the spurious oscillations have no effect on velocity and velocity-derived fields. They do, however, preclude determining a raw pressure field from the computed solution. A number of options for filtering or otherwise eliminating these spurious oscillations have been proposed [15,18]. Since the spurious oscillations stem from the highest-order polynomial, T_{N_x} or T_{N_y}, a post-processing step is performed in the present work in which the correct pressure-gradient information in the domain interior is used to reconstruct a two-dimensional Chebyshev interpolant for pressure of order lower than the original expansion, viz. of order $(N_x - 2) \times (N_y - 1)$. This 'filtering' operation does degrade the pressure solution somewhat, but is relatively straightforward to implement and does suppress the spurious oscillations.

4. RESULTS AND DISCUSSION

4.1. The full-domain case

The results with two grids, both with two domains but with two different values of (N_x, N_y) = (90, 12), and (100, 18), are presented. The grid (nodes) corresponding to $N_x = 90$ and $N_y = 12$ is shown in Figure 1. The Gauss–Lobatto Chebyshev collocation points are clustered at the ends of the domain, with points in the central region being relatively widely spaced. From a conventional perspective, this might appear to imply that the resolution is coarse in the central region, but because of its global nature, this is not the case when a spectral method is used. Further, the minimum separations between adjacent grid points are 0.0091 and 0.0085 (minimum Δx and Δy respectively), which might be compared with the corresponding values, ≈ 0.05 and ≈ 0.01, for the finest grid in the spectral element solution in G93. In spite of the much larger (by approximately a factor of four) total number of nodes in the fine grid spectral element solution, the minimum separations in the present work are smaller, a heuristic indication of the finer resolution in the present work [9].

Contours of the streamfunction (Φ), the vorticity (ω), the pressure (p), and the local divergence ($\nabla \cdot \mathbf{u}$) obtained with the 90×12 grid are shown in Figure 2 for the domain up to $x = 12$. The contours were constructed by spectrally interpolating the solution at the irregularly spaced collocation nodes to a regular grid with uniform $\Delta x = 0.03$ and $\Delta y = 0.0125$. As expected, two regions of flow separations are found, one separating at the step and reattaching at the lower boundary, and the other separating and reattaching at the upper boundary. The overall smooth contours of these key variables indicate that the solution obtained is generally well-behaved, although some difficulty in the immediate vicinity of the step will be evident below. The absence of cells characteristic of spurious pressure oscillations in the pressure solution shows that these have been successfully suppressed by the post-processing filtering and reconstruction operation. Further, the maximum local divergence is $O(10^{-10})$, which occurs at the boundaries of the subdomains, as is typical of spectral solutions.

Various standard measures are used to compare numerical predictions of the BFS flow, including the locations of the separation (denoted x_s) and reattachment (denoted x_r) points, and the values of the Φ and ω at local extremes of Φ, termed vortex centers [4] (and so denoted here as (x_v, y_v) or x_v). Characteristics on the lower boundary are denoted with an l subscript, and those on the upper boundary with a u subscript. The present results are compared in Table I with those of Gartling [4] and others reported in G93. Separation and reattachment points were identified as points of zero shear stress ($= \partial u/\partial y$), while extremes in Φ were found by simple manual search. Again, spectral interpolation was used throughout in these evaluations. The term 'grid-independence' is relative; a difference in the fourth or fifth significant figure is seen in a comparison of the results using the two grids. For most purposes, the results of the 90×12 grid may be termed grid-independent as far as the prediction of these standard measures are concerned, in spite of slight wiggles in the ω, (and also p) contours near the step. The agreement at both resolutions with the results of Gartling is generally excellent. The estimated locations of the vortex centers differ, but this is attributed to the flat variation of Φ in the vicinity of the centers, the difference in Φ between the center according to Gartling and the centers estimated here being $O(10^{-5})$, even though the locations change in the second decimal place. Table I also shows that the values of Φ, and ω, at the Gartling vortex centers (denoted $(x_v)_G$) are in excellent agreement. The present solution generally agrees more closely with the results of Gartling than with those of the finite difference streamfunction/vorticity solution (FD) *except* with respect to the locations of the vortex centers and the values of Φ and ω.

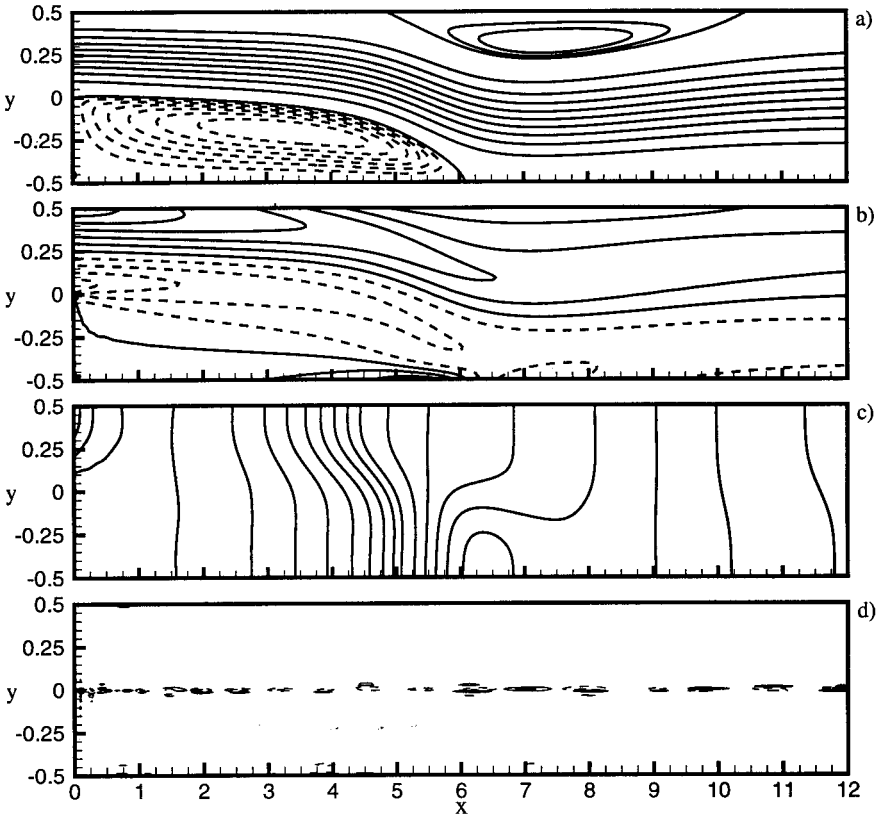

Figure 2. Contours of flow characteristics up to $x = 12$ derived or obtained from full-domain computations: (a) Φ, (b) ω, (c) p and (d) divergence ($\nabla \cdot \mathbf{u}$) obtained with the 90×12 grid. Contour levels are set at the same levels as in Gartling [4], except for $\nabla \cdot \mathbf{u}$, for which the levels are $\pm 1 \times 10^{-11}$, $\pm 3 \times 10^{-11}$ and $\pm 5 \times 10^{-11}$. Dashed lines indicate negative values.

The total number of nodes or grid points used in the present work is significantly smaller than that of previous stable simulations, and, for the 90×12 grid, is even smaller than the total number of nodes used in the Kaiksis *et al.* [1] simulations (= 2700 nodes), that are known to be inadequately resolved. A 90×10 grid with a total of 1911 nodes still yielded a convergent steady solution, yet a simulation with a larger total number of nodes, namely with a 80×12 grid (2025 nodes), failed to converge to a steady state, i.e. the difference between solutions at the two different times did not decay with time. Thus, while the resolution in the y-direction is already adequate with $N_y = 10$, a resolution of $N_x > 80$ is necessary; the asymptotic exponential accuracy may only be achieved beyond a minimum number of nodes [9,15]. At least in a transient simulation, the streamwise resolution may be more important than might be at first thought, because small features are generated during the simulation, eventually disappearing at the steady state.

Transverse profiles of Φ, ω, and p are plotted in Figure 3 at four stations, $x = 0$, 1, 4 and at 7. Except for the inlet ω profile, these generally exhibit a smooth variation across the subdomain boundary. The wiggles in the inlet ω profile are due to the discontinuity in $\partial u/\partial y$ at the inlet plane. Except for the ω at the inlet plane, the solutions for Φ and ω at the two resolutions are visually identical. A slight difference in p is due to a constant difference in the reference pressure. A more detailed comparison of point values at $x = 7$ with the benchmark

results is given in Table II. For both resolutions, the agreement between the present and the benchmark results for u is as before, excellent. The agreement deteriorates slightly in the case of ω, with better agreement between the present results at the two resolutions than with the benchmark results. At this level of agreement in the primitive variables, it is not clear whether the benchmark or the present solution is the more accurate, since ω is a derived result, and some error might have been made in the benchmark solution in computing derivative quantities from the raw solution of the primitive variables. The largest differences are found in a comparison of the pressure, where an absolute difference of ≈ 0.008 or $\approx 5\%$ is seen. Gartling [4] noted that the pressure in incompressible flows is a very sensitive variable, and a comparison of his mesh C and mesh E (the finest grid) results still showed a noticeable difference (≈ 0.005) at the inlet plane, such that grid-independence, at least for the pressure solution, may not have been completely achieved. This also holds for the present computations with the difference between the results at the two resolutions (≈ 0.0019 or $\approx 1\%$) being entirely attributable to the difference in reference pressure. On the other hand, the weak singularity at the step is likely to have had an impact on the spectral solution. The pressure differences away from the step region are however, accurately computed; the difference in

Table I. Comparison of present results on characteristic flow parameters with previously published results

Quantity	I	II	GC	GE	FD	SE
$(x_r)_l$	6.0970	6.0964	6.09	6.10	6.082	6.10
$(x_s)_u$	4.8534	4.8534	4.85	4.85	4.8388	4.86
$(x_r)_u$	10.4811	10.4785	10.48	10.48	10.4648	10.49
$(x_v)_l$	3.414	3.392	3.350	3.350	3.375	n/a
$(y_v)_l$	−0.205	−0.204	−0.200	−0.200	−0.2032	n/a
$(x_v)_u$	7.439	7.447	7.400	7.400	7.4375	n/a
$(y_v)_u$	0.315	0.315	0.300	0.300	0.3125	n/a
$\Phi(x_v, y_v)_l$	−0.03420	−0.03420	n/a	n/a	0.034195	−0.0342
$\omega(x_v, y_v)_l$	−2.2623	−2.2620	n/a	n/a	n/a	n/a
$\Phi((\mathbf{x}_{vl})_G)$	−0.03418	−0.03419	−0.0342	−0.0342	−0.034195	−0.0342
$\omega((\mathbf{x}_{vl})_G)$	−2.2776	−2.2822	−2.285	−2.283	n/a	n/a
$\Phi(x_v, y_v)_u$	0.50652	0.50653	n/a	n/a	0.50661	0.5065
$\omega(x_v, y_v)_l$	1.1474	1.1527	n/a	n/a	n/a	n/a
$\Phi[(\mathbf{x}_{vu})_G]$	0.50639	0.50639	0.5064	0.5064	n/a	n/a
$\omega[(\mathbf{x}_{vu})_G]$	1.3199	1.3212	1.321	1.322	n/a	n/a
Nodes	2275	3737	32 841	129 681	(1920×128)	$\gtrapprox 8000$

1. In this and Table II, I and II refer to the present results using the grids ($N_x = 90$, $N_y = 12$) and ($N_x = 100$, $N_y = 18$) respectively.
2. GC and GE refer to the results of Gartling [4] on mesh C and on mesh E respectively, using biquadratic velocity and linear discontinuous pressure elements to solve the steady problem.
3. FD refers to results reported in G93 obtained from a transient simulation with a finite difference (centered differences) solution of the equations in a streamfunction/vorticity formulation. The domain was substantially shortened so the grid given above extended only up to $x = 15$, and the time integration was performed up to $t = 400$.
4. SE refers to results reported in G93 obtained from a transient simulation with a spectral element approach presumably on the finest grid, namely 136 elements with either $N_x = N_y = 8$ for a total of 9009 nodes. These computations were actually done for a slightly longer channel, up to $x = 34$; for a channel up to $x = 30$, the total number of nodes would be reduced by approximately 10%, yielding the approximate estimate given in the table. The time integration was performed to $t = 200$ and results extrapolated.

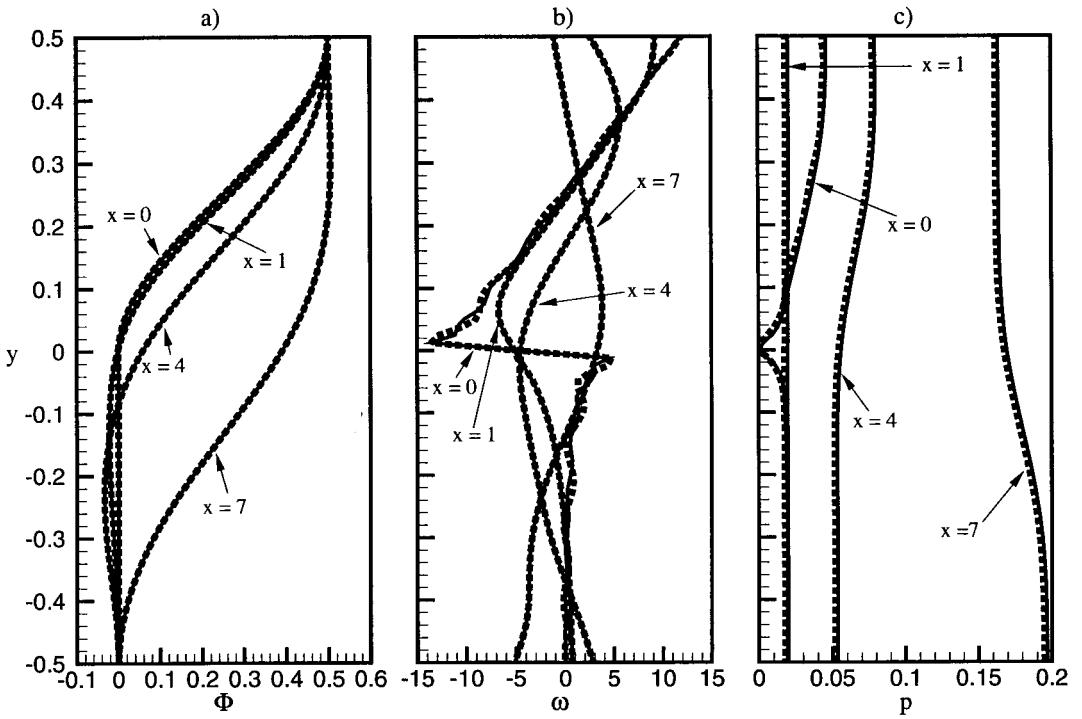

Figure 3. Comparison of profiles of characteristic flow quantities derived or obtained from full-domain computations with different grids: (a) Φ, (b) ω and (c) p, at different sections ($x = 0$, 1, 4, 7). Solid lines obtained from 100×18 grid and symbols obtained from 90×12 grid.

pressure between the top and the bottom at $x = 7$ in both the present solutions and the benchmark solution agree to less than 1%.

These results show that, in spite of the presence of the weak singularity at the step, which would be much milder if an upstream section would have also been simulated, accurate and stable steady state solutions for $Re = 800$ can be obtained with a spectral domain decomposition approach, with a substantially smaller number of nodes than used in previous work. Whether 'exponential' rates of convergence were achieved, at least in regions where the flow solution is smooth, would require more exhaustive simulations. In terms solely of the total number of nodes required for a given resolution, the strategy of increasing the order of the basis polynomial is much more effective than increasing the number of subdomains. This is expected for smooth solutions, since the accuracy of spectral methods increases exponentially with the order of the approximating polynomial, while increasing the number of subdomains for the same number of total nodes only results in an algebraic improvement. In a study of Stokes flow in a cavity [13], it was concluded that single-domain spectral simulations were 'vastly more accurate' than multidomain simulations for given matrix size. Interestingly, for the same BFS flow, G93 also reported on a comparison between finite element solutions with elements of different order, and concluded that many more lower-order (bilinear) elements were needed for the same accuracy achieved by the higher-order (biquadratic) elements. While overall computational effort may be influenced by other algorithmic issues, e.g. the efficient solution of the resulting linear system and parallelization/vectorization of the algorithm, than

solely the number of nodes, the large (at least a factor of two) reduction in the number of nodes makes the spectral approach much more attractive. Users of spectral domain decomposition methods should therefore, weigh carefully the undoubted advantages of domain decomposition, but should not automatically adopt the strategy of increasing the number of subdomains as the only feasible way of increasing the resolution.

4.2. The short-domain case

In all computations for the short-domain case, with outlet at $x = 7$, two subdomains were used with $N_x = 50$ and $N_y = 12$ in each domain. Because only a single subdomain is used in the x-direction, the streamwise locations of the nodes in a spectral solution for the short-domain case necessarily differ from the locations for the full-domain case. The choice of $N_x = 50$ ensures that streamwise nodal density is higher than that used in the full-domain case. Rather surprisingly, the zero normal gradient outflow condition yields a qualitatively erroneous but still stable and convergent solution, with no separation on the upper boundary and no reattachment on the lower boundary within the shortened domain. The contours of relevant variables obtained using the zero normal gradient condition (Figure 4) do not exhibit any otherwise anomalous behavior, except possibly a slight wiggle in the pressure contours at the outflow boundary. The present results contrast with results (reviewed in [8]) obtained with finite volume approaches, where good agreement was apparently obtained with this condition.

Because of the use of Gauss–Lobatto points, the spectral method using Chebyshev polynomials necessarily clusters points near the boundaries of each subdomain, and, in particular, near the outlet. The organizers of the OBC symposium [8] specified that no extra fine meshes be used near the outlet, presumably because the effects of the OBC would thereby be limited

Table II. Comparison of full-domain solution at $x = 7$ at different resolutions and with the benchmark

y	u			p			ω		
	I	II	Gartling	I	II	Gartling	I	II	Gartling
0.50	0.0000	0.00000	0.000	0.1622	0.1641	0.1562	−1.0342	−1.0323	−1.034
0.45	−0.03817	−0.03814	−0.038	0.1623	0.1641	0.1562	−0.4928	−0.4917	−0.493
0.40	−0.04890	−0.04892	−0.049	0.1623	0.1641	0.1562	−0.06317	0.06310	0.061
0.35	−0.03162	−0.03154	−0.032	0.1623	0.1641	0.1562	0.6372	0.6385	0.635
0.30	0.01519	0.01516	0.015	0.1622	0.1641	0.1562	1.2481	1.2430	1.237
0.25	0.09320	0.09300	0.092	0.1623	0.1641	0.1562	1.8937	1.8939	1.888
0.20	0.2043	0.2042	0.204	0.1624	0.1642	0.1563	2.5847	2.5867	2.588
0.15	0.3494	0.3494	0.349	0.1627	0.1646	0.1567	3.2517	3.2498	3.267
0.10	0.5232	0.5231	0.522	0.1635	0.1654	0.1574	3.7185	3.7191	3.751
0.05	0.7101	0.7100	0.709	0.1651	0.1669	0.1590	3.7743	3.7775	3.821
0.00	0.8862	0.8861	0.885	0.1677	0.1695	0.1615	3.3062	3.3038	3.345
−0.05	1.0248	1.0247	1.024	0.1713	0.1732	0.1652	2.3363	2.3302	2.362
−0.10	1.1055	1.1055	1.105	0.1758	0.1777	0.1697	1.0306	1.0326	1.046
−0.15	1.1178	1.1177	1.118	0.1807	0.1825	0.1746	−0.3667	−0.3678	−0.374
−0.20	1.0618	1.0618	1.062	0.1852	0.1871	0.1792	−1.6685	−1.6654	−1.684
−0.25	0.9476	0.9477	0.948	0.1891	0.1909	0.1831	−2.6916	−2.6921	−2.719
−0.30	0.7915	0.7916	0.792	0.1919	0.1938	0.1859	−3.3615	−3.3602	−3.392
−0.35	0.6124	0.6126	0.613	0.1937	0.1955	0.1876	−3.6412	−3.6420	−3.658
−0.40	0.4270	0.4271	0.428	0.1946	0.1964	0.1885	−3.7169	−3.7173	−3.687
−0.45	0.2318	0.2319	0.232	0.1949	0.1968	0.1888	−4.1660	−4.1680	−4.132
−0.50	0.0000	0.0000	0.000	0.1950	0.1969	0.1889	−5.1520	−5.1517	−5.140

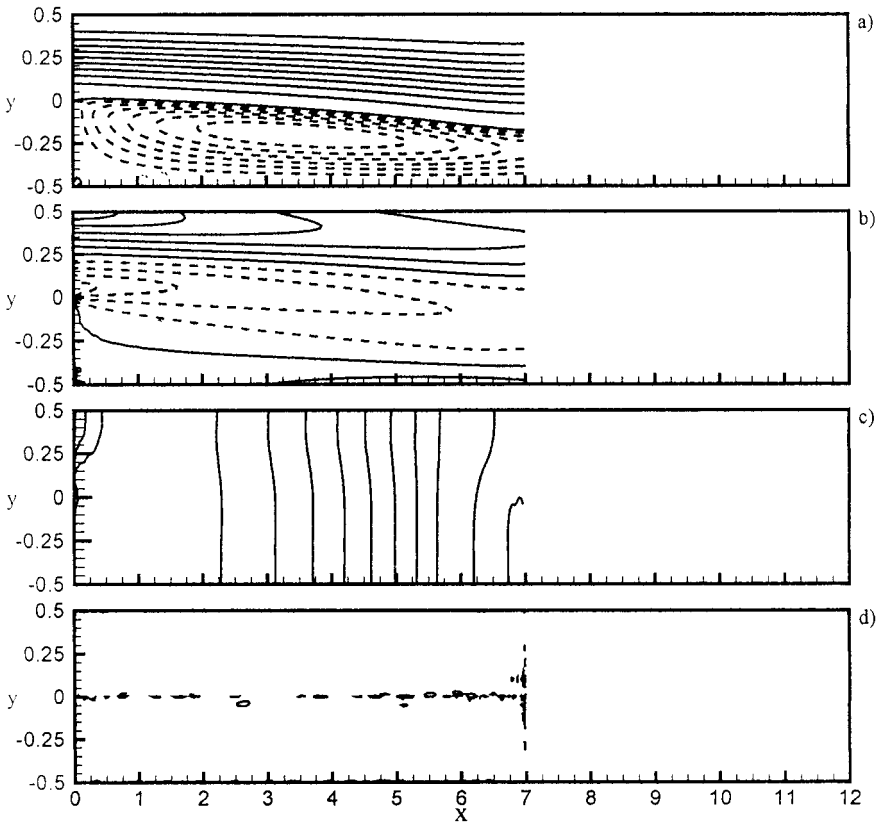

Figure 4. Contours of flow characteristics derived or obtained with the 50×12 grid in the shortened domain with the zero normal gradient outflow boundary condition: (a) Φ, (b) ω, (c) p and (d) divergence ($\nabla \cdot \mathbf{u}$). Contour levels are the same as in Figure 2.

by more local finite differences or finite element approaches. The present results with the zero normal gradient OBC are possibly all the more surprising, but indicate again that node clustering in spectral methods is not necessarily associated with localization. Rather, the high-order of the polynomial expansion and the use of a single subdomain in the x-direction result in greater sensitivity and more global effect of the OBC.

In spite of differences ($O(3–4\%)$) for the separation and reattachment points, the results shown in Table III using the pseudo stress-free condition must seem remarkably good compared with the notably poor performance of the zero normal gradient condition. Also shown in Table III are results of a finite element computations [5] for the same pseudo stress condition, which differ significantly from the present as well as the benchmark results, and would seem to imply a quite poor performance of this condition. The difference is attributed to coarseness of the mesh and the use of lower-order elements, and illustrates the danger of comparing only short-domain solutions with the benchmark full-domain solutions without first comparing full-domain solutions. Much closer agreement for the short-domain solution is found with a finite difference streamfunction/vorticity solution reported in G93, though with a different boundary condition.

Table III. Comparison of the present full- and short-domain results on basic flow characteristics using the pseudo stress-free condition with previous short-domain results reviewed in [8]

Quantity	Present results		FE	FD
	Short-domain	Full-domain	Short-domain	
$(x_r)_l$	5.905	6.097	5.578	5.86
$(x_s)_u$	4.682	4.853	4.29	4.636
$(x_v)_l$	3.361	3.414	2.90	3.328
$(y_v)_l$	−0.205	−0.205	−0.325	−0.203
$\Phi(x_v, y_v)_l$	−0.03415	−0.03420	−0.0314	−0.03412
$\omega(x_v, y_v)_l$	−2.271	−2.262	−2.46	−2.285

1. The FE short-domain was obtained using a 42×20 mesh, bilinear velocity and piecewise constant pressure elements with the pseudo stress-free outflow condition.
2. The FD short-domain was obtained with the same code as that described in Table I.
3. Results for the vortex center associated with the upper recirculation region from the short-domain computations are not shown because vorticities were still increasing towards the outflow boundary.

5. SUMMARY

The steady laminar backward-facing step flow at a Reynolds number of 800, based on channel height, was studied using a spectral domain decomposition approach, emphasizing the satisfaction of the incompressibility constraint. Stable convergent solutions were obtained with substantially fewer nodes than in previously reported work by increasing the order of the polynomial expansion and minimizing the number of subdomains. Excellent agreement in terms of the velocity field and the characteristics of the flow was achieved with the benchmark solution. The greater sensitivity of spectral methods to boundary conditions was also exploited in studying the effect of two different, but widely used, sets of outflow boundary condition: the zero normal gradient and the pseudo stress-free conditions. The latter was found to be much more robust than the former, which resulted in a qualitatively erroneous solution.

ACKNOWLEDGMENTS

The comments of the editor and the reviewers helped in clarifying a number of issues. This research was partially supported through the Purdue Research Foundation.

REFERENCES

1. L. Kaiktsis, G.E. Karniadakis and S.A. Orszag, 'Onset of three-dimensionality, equilibria, and early transition in flow over a backward-facing step', *J. Fluid Mech.*, **231**, 501–528 (1991).
2. A.W. Runchal, 'ANSWER: A benchmark study for backward-facing step', in: B. Blackwell and D.W. Pepper (eds.), *Benchmark Problems for Heat Transfer Codes*, Winter Annual Meeting ASME, Anaheim, CA, 1992, pp. 13–20.
3. D. Choudhury, 'A numerical study of laminar flow and heat transfer in a backward-facing step using FLUENT: a finite volume code', in: B. Blackwell and D.W. Pepper (eds.), *Benchmark Problems for Heat Transfer Codes*, Winter Annual Meeting ASME, Anaheim, CA, 1992, pp. 53–59.
4. D.K. Gartling, 'A test problem for outflow boundary conditions—flow over a backward-facing step', *Int. J. Numer. Methods Fluids*, **11**, 953–967 (1990).
5. P.M. Gresho, D.K. Gartling, J.R. Torczynski, K.A. Cliffe, K.H. Winters, T.J. Garratt, A. Spence and J.W. Goodrich, 'Is the steady viscous incompressible two-dimensional flow over a backward-facing step at $Re = 800$ stable?', *Int. J. Numer. Methods Fluids*, **17**, 501–541 (1993).

6. J.R. Torczynski, 'A grid-refinement study of two-dimensional transient flow over a backward-facing step using a spectral element method', *Separated Flows*, *ASME Fluids Eng. Div.*, **149**, 1–7 (1993).
7. H.C. Ku, R.C. Hirsh, T.D. Taylor and A.P. Rosenberg, 'A pseudo spectral matrix element method for solution of three-dimensional incompressible flows and its parallel implementation', *J. Comp. Phys.*, **83**, 260–291 (1989).
8. R.L. Sani and P.M. Gresho, 'Resume and remarks on the open boundary condition mini-symposium', *Int. J. Numer. Methods Fluids*, **18**, 983–1008 (1994).
9. D. Gottlieb and S.A. Orszag, *Numerical Analysis of Spectral Methods*, SIAM, Philadelphia, PA, 1977.
10. T.A. Zang, 'On the rotation and skew-symmetric forms for incompressible flow simulations', *Appl. Numer. Math.*, **7**, 27–40 (1991).
11. P.M. Gresho and R.L. Sani, 'On pressure boundary conditions for the incompressible Navier–Stokes equations', *Int. J. Numer. Methods Fluids*, **7**, 1111–1145 (1987).
12. D. Gottlieb and C.L. Streett, 'Quadrature imposition of compatibility conditions in Chebyshev methods', *J. Sci. Comp.*, **5**, 223–239 (1990).
13. M.R. Schumack, W.W. Schultz and J.P. Boyd, 'Spectral method solution of the Stokes equations on non-staggered grids', *J. Comp. Phys.*, **90**, 30–58 (1991).
14. P.M. Gresho, 'Some current CFD issues relevant to the incompressible Navier–Stokes equations', *Comp. Methods Appl. Mech. Eng.*, **87**, 201–252 (1991).
15. C. Canuto, M.Y. Hussaini, A. Quarteroni and T.A. Zang, *Spectral Methods in Fluid Dynamics*, Springer, New York, 1988.
16. A.J. Chorin, 'Numerical solution of the Navier–Stokes equations', *Math. Comp.*, **22**, 742–762 (1968).
17. P.M. Gresho and S.T. Chan, 'On the theory of semi-implicit projection methods for viscous incompressible flow and its implementation via finite element method that also introduces a nearly consistent mass matrix. Part 2: Implementation', *Int. J. Numer. Methods Fluids*, **11**, 621–659 (1990).
18. T.N. Phillips and G.W. Roberts, 'The treatment of spurious pressure modes in spectral incompressible flow calculations', *J. Comp. Phys.*, **105**, 150–164 (1993).

